

Cross-Calibration of TIMED SEE and SOHO EIT Irradiances

R.A. Hock · F.G. Eparvier

Received: 16 November 2007 / Accepted: 6 May 2008 / Published online: 30 May 2008
© Springer Science+Business Media B.V. 2008

Abstract Absolutely calibrated solar images are necessary for a variety of solar physics problems, such as the identification of solar variability sources and the derivation of differential emission measure (DEM) maps. SOHO EIT is absolutely calibrated by using TIMED SEE spectra to provide a method of determining physical values of irradiance for EIT images. EIT images from 1 April 2002 to 15 March 2005 in the 28.4- and 30.4-nm channels are compared to SEE daily spectra from the same time period. The resulting fitted EIT irradiances are well correlated to SEE irradiance measurements and are within the uncertainties of both instruments. The new cross-calibration results are compared to the currently used calibration based on the UARS SUSIM Mg II index.

Keywords Solar EUV irradiance

1. Introduction

Identification of sources of solar variability, the calculation of differential emission measure (DEM) maps, and other solar physics problems depend upon absolutely calibrated solar images. *Solar and Heliospheric Observatory* (SOHO) Extreme ultraviolet Imaging Telescope (EIT) images the transition region and lower corona of the Sun in four channels in the extreme ultraviolet (EUV) with a wide bandpass (FWHM \approx 1.0 nm). Although all EIT images are relatively calibrated to the first EIT images taken on 1 February 1996 by using visible-light flatfields and the Solar Ultraviolet Spectral Irradiance Monitor (SUSIM) Mg II index (Clette *et al.*, 2002; Floyd *et al.*, 2005), an absolute calibration is more difficult to obtain. The wide bandpasses allow multiple emission lines formed at different temperatures to be imaged simultaneously. Particularly in the EUV, the relative strength of these different lines varies considerably over time. This variability makes it nearly impossible to convert from pixel counts to physical units without knowing the solar spectrum.

R.A. Hock (✉) · F.G. Eparvier
Laboratory for Atmospheric and Space Physics, University of Colorado, Boulder, CO 80303, USA
e-mail: rachel.hock@lasp.colorado.edu

The solar spectrum can be derived by using a DEM and a spectral database such as CHIANTI. CHIANTI provides a database of atomic data that can be used to calculate optically thin emission lines. Although CHIANTI is available even when real solar data is not, there are disadvantages in using a DEM. A DEM is only a theoretical calculation of the solar spectrum. CHIANTI, for example, is unable to model the optically thick He II line at 30.4 nm that dominates one of the EIT channels. Other lines may not be modeled adequately, and not all possible atomic lines are in the spectral database. A DEM might also not be able to capture all solar variability as it uses proxies from other parts of the solar spectrum, which vary differently than the EUV.

A better way to calibrate EIT images would be to use accurate solar EUV spectra convolved with the EIT spectral responsivities. Since the 1980s, solar irradiance measurements have been sporadic in the EUV. However, after its launch in late 2001, the NASA *Thermosphere Ionosphere Mesosphere Energetics and Dynamics* (TIMED) mission's Solar Extreme ultraviolet Experiment (SEE) has made daily spectral measurements of the EUV that overlap with those taken by the SOHO mission. During the five years of its mission, SEE has observed both high and low levels of solar activity that compare well with previous EUV measurements. Woods *et al.* (2005) show that SEE version 8 data are consistently 20% lower than the SOHO SEM 26–34 nm band and in good agreement at 0–50 nm (and version 9 is in better agreement).

The primary goal of this work is to provide an absolute calibration of EIT images by using daily SEE irradiance measurements. In addition to providing physical units for EIT images, this cross-calibration will correct for long-term changes in the CCD. When the NASA *Solar Dynamics Observatory* (SDO) launches in 2008, we are planning to apply this technique to Atmospheric Imaging Assembly (AIA) solar images using solar EUV irradiance measurements from the Extreme-ultraviolet Variability Experiment (EVE).

This paper provides an introduction to the EIT and SEE instruments, discusses the data analysis and cross-calibration steps, gives the results of the cross-calibration, and concludes with implications for future work.

2. Data

2.1. EIT Images and Image Processing

SOHO EIT images the Sun in four channels in the EUV centered on 17.1, 19.5, 28.4, and 30.4 nm with a wide bandpass of 1.5–2.0 nm FWHM. The EIT instrument is a normal-incidence, multilayer telescope that provides wide-field images of the Sun out to $1.5R_{\odot}$ with a 1024×1024 pixel CCD (Dere *et al.*, 2000).

For this cross-calibration, we use EIT images from 1 April 2002 to 15 March 2005 to overlap with TIMED SEE. On average, EIT takes four full field-of-view images in each of the four wavelength bands per day during the Full Sun observing campaign. Furthermore, the Coronal Mass Ejection (CME) Watch observing campaign takes additional full images in the 19.5-nm band. Owing to SEE's moderate spectral resolution shortward of 27 nm (see Section 2.2), only the 28.4- and 30.4-nm channels are used in this study. In total, over 10 000 EIT images from these two channels were used in the cross-calibration.

The raw EIT images are processed by using the EIT SolarSoftWare program `eit_prep.pro` (Clette *et al.*, 2002). This IDL program reads in the raw FITS image and corrects for both the dark current and flatfield. In addition, processing removes particle hits, normalizes the exposure time to 1 second, and corrects time response changes (discussed next). For this

analysis, a further step is added to normalize the counts to 1 AU. This normalization allows for a direct comparison with the SEE irradiance data that are also normalized to 1 AU.

EIT images are calibrated for time response changes in two steps (Clette *et al.*, 2002). The first uses visible lamp flatfields to track the degradation of each pixel, which is proportional to its EUV exposure. The areas of the CCD that image low latitudes of the Sun, where there is more solar activity, degrade faster than the areas of the CCD that image far from the solar equator. Occasionally when SOHO is not pointing at the Sun, EUV flatfields are taken by offsetting the Sun at many positions and are used to determine the relationship between the CCD's response to visible and EUV light.

The second calibration uses the SUSIM chromospheric Mg II index to track the overall long-term degradation. By assuming a relationship between the index and EIT, EIT images can be normalized to the first EIT images taken on 1 February 1996 (Floyd *et al.*, 2005). The Mg II index, which measures the core-to-wing ratio of the Mg II feature at 279.9 nm, is inherently free of degradation and is a convenient proxy for the chromosphere. For this analysis, the Mg II index correction was left out of the processing steps. As the EIT bandpasses contain coronal and transition region emissions that do not necessarily trend the same as chromospheric lines, the Mg II index is not expected to be the best proxy for correcting the long-term degradation. The SEE irradiance can correct for the long-term degradation in addition to providing physical units for the EIT images. Since SEE data are direct EUV measurements, the cross-calibration should be better than a correction made using a proxy model.

Furthermore, EIT undergoes periodic bakeouts to improve the CCD sensitivity. During a bakeout, the CCD is heated to 18°C. The bakeouts attempt to undo (1) the deposition of contaminants on the CCD window that absorb the UV photons before they hit the detector and (2) the reduction of charge collection efficiency (CCE) from EUV-induced and particle-induced damage in the CCD itself (Newmark *et al.*, 2000). Since May 2003, the bakeouts occurred more frequently and last longer as the high gain antenna (HGA) has been forced to remain fixed. As a result, the SOHO spacecraft periodically enters "keyhole periods" where it cannot point both the instruments at the Sun and the HGA at the Earth. During these periods, EIT is unable to transmit data, so to utilize the downtime, it undergoes a bakeout. These bakeouts do restore sensitivity and improve the quality of the images. However, the CCD degrades the fastest right after a bakeout. This means that the EIT CCD response is a sawtooth pattern, as seen later in Figure 2.

2.2. SEE Irradiance Measurements

TIMED SEE is an experiment designed to accurately and precisely measure the full-disk solar vacuum ultraviolet (VUV) irradiance and its variability (Woods *et al.*, 2005). It has been operating since January 2002 and has two instruments: The EUV Grating Spectrograph (EGS) covers the EUV and FUV from 26 to 194 nm with 0.4-nm resolution, and the soft X-ray (XUV) region from 0.1 to 35 nm is covered by the XUV Photometer System (XPS) using 12 photodiodes with bandpasses from 5 to 10 nm. EGS is a 1/4-meter Rowland circle spectrograph with a mechanically ruled concave grating and a microchannel plate detector with a two-dimensional 1024×64 coded anode (CODACON) readout. SEE observes the Sun for 3 minutes every orbit (97 minutes) and takes on average 14–15 solar observations a day. The data are calibrated and corrected for degradation by using sounding rocket underflights plus internal flatfield lamps (EGS) and redundant on-board channels (both instruments). The data also are normalized to 1 AU. Data products are available with either 0.1- or 1.0-nm resolution and either as an observation average or a daily average that removes solar flares.

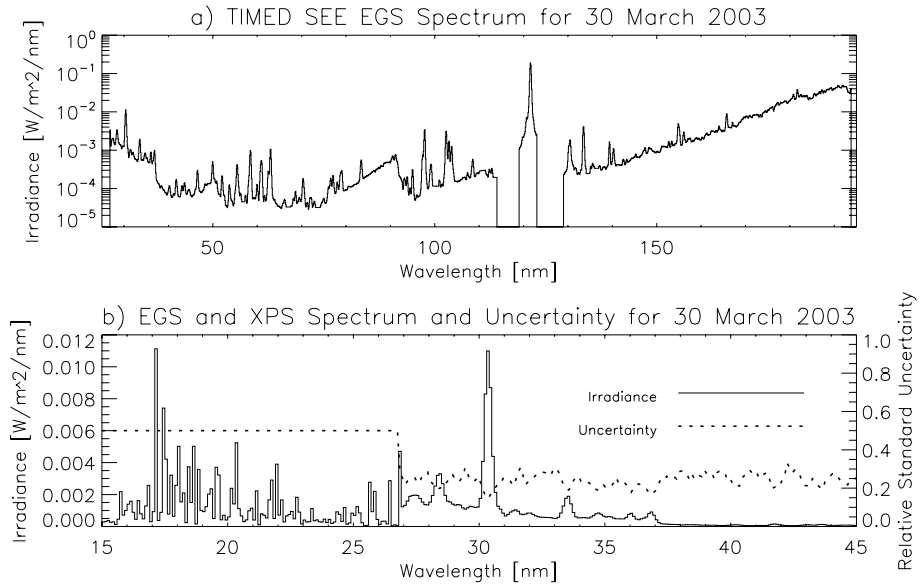


Figure 1 (a) Sample EGS level 2 spectrum covering 26 to 194 nm. (b) Combined EGS level 2 and XPS level 4 spectra covering 15 to 45 nm with 0.1-nm sampling.

The SEE data product used for this comparison to EIT is a combination of the XPS level 4 and the EGS level 2, version 9 (available online at <http://lasp.colorado.edu/see/>). The EGS level 2 product is the daily average irradiance on a 0.1-nm grid of solar spectra from the EGS instrument (26 to 194 nm) (Figure 1(a)). Although a higher time resolution product exists, the daily average is used to decrease errors from detector photon counting statistics. The EGS level 2 product has a relative standard uncertainty that varies from 30% to 40% throughout most of its range (Figure 1(b)).

The wavelengths shorter than 26 nm are covered by the XPS level 4 data product (Figure 1(b)). This uses a CHIANTI spectrum from 0 to 40 nm scaled to the broadband measurements from the XPS photodiodes. As the XPS level 4 is a model spectrum, its spectral accuracy is estimated to be about 50%. This product is also a daily average irradiance scaled on a 0.1-nm grid. Whereas XPS measurements are only broadband, the CHIANTI model scaled to the photodiode signal allows us to cover the full range of the EIT bandpasses for the 28.4- and 30.4-nm channels. The shorter wavelength EIT images (17.1 and 19.5 nm) are not studied here as the majority of their bandpasses lie within the more uncertain XPS spectral range.

Since the last sounding rocket flew in late 2004, this study limits the cross-calibration to April 2002 through March 2005 to ensure that the best SEE data are used.

3. Cross-Calibration

The cross-calibration calculates the time-dependent calibration factor to provide physical units for the brightness of SOHO EIT images. This is done by comparing the brightness or total corrected counts of processed EIT images with the irradiance from TIMED SEE at the same wavelengths.

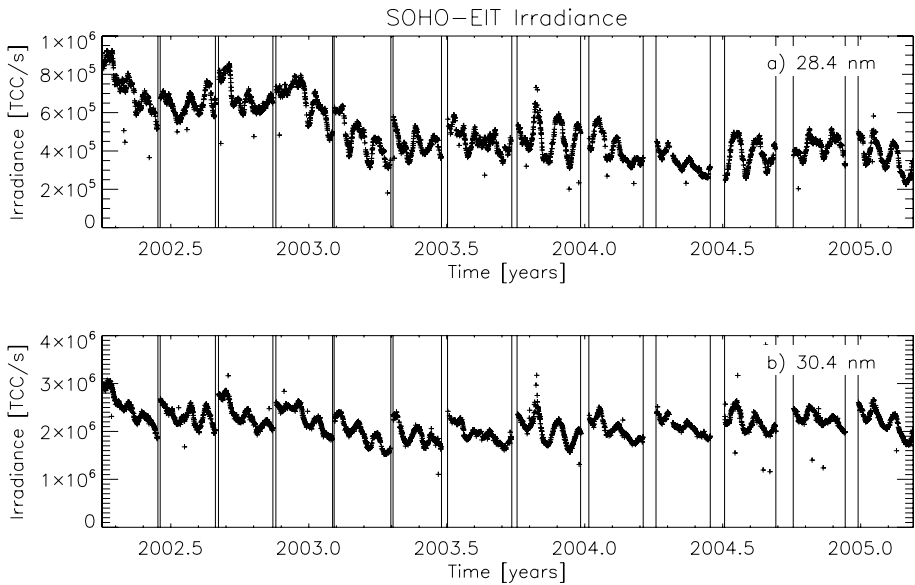


Figure 2 Time series of EIT total corrected counts (TCC) for (a) the 28.4-nm channel and (b) the 30.4-nm channel. The vertical lines mark the start and end of EIT bakeouts.

3.1. EIT Irradiance

The irradiance from the EIT images is calculated after the raw images have been processed (see Section 2.1) by totaling the corrected counts from each pixel. This gives a total corrected counts (TCC) with units of counts s^{-1} as the images have already been normalized to 1 second. All the pixels from an image, including those off the solar disk, are used as SEE has a larger field of view than EIT and there are EUV emissions from the corona that appear off the solar disk. Figure 2 shows the time series of TCC for 28.4- and 30.4-nm images. The sawtooth pattern, particularly evident in the 30.4-nm time series, is due to the change in CCD sensitivity after bakeouts.

3.2. SEE Irradiance

By convolving the SEE irradiance data with the normalized EIT spectral responsivities we can calculate the expected calibrated EIT measurement. The EIT spectral responsivities are given by the SolarSoftWare routine `eit_params.pro` (Dere *et al.*, 2000) and are normalized so that the total area under the responsivity is unity (Figure 3). To calculate the expected EIT measurement, E , the SEE irradiance spectrum, F_{SEE} , is convolved with the normalized EIT response, R_{EIT} , by using

$$E = \int_{\lambda_1}^{\lambda_2} F_{\text{SEE}}(\lambda) \cdot R_{\text{EIT}}(\lambda) \cdot d\lambda, \quad (1)$$

where λ_1 and λ_2 are the range of the SEE data. Figure 4 shows the time series of the SEE irradiance convolved with the normalized EIT responsivity for 28.4 and 30.4 nm and the associated uncertainties.

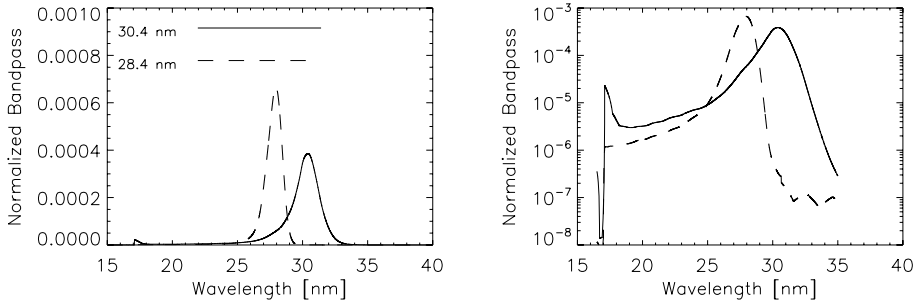


Figure 3 Normalized EIT bandpasses for the 28.4- and 30.4-nm channels from the SolarSoftware eit_prep.pro on linear (left) and logarithmic (right) scales.

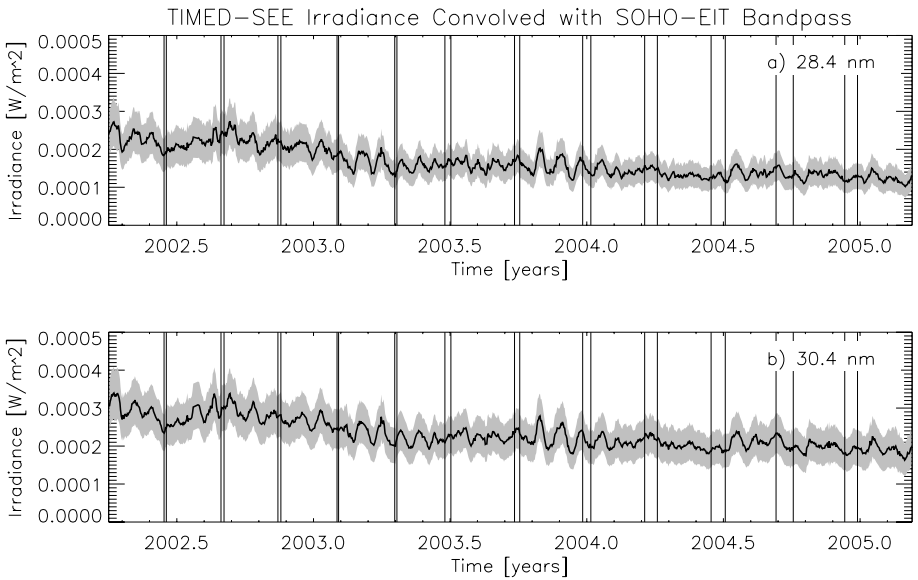


Figure 4 Time series of SEE irradiance convolved with (a) EIT 28.4-nm and (b) EIT 30.4-nm responsivities. The vertical lines mark the start and end of EIT bakeouts. The shaded areas are the SEE uncertainty.

3.3. Ratio of EIT to SEE

The absolute calibration of EIT is determined by performing a least-squares fit of the ratio of the EIT TCC and the convolved SEE irradiance (Figure 5). Since we exclude the Mg II index correction when we process the EIT images, the EIT TTC is not corrected for changes to the CCD sensitivity across bakeout periods, as evident in Figure 2. The absolute calibration is therefore both correcting for long-term changes in the CCD and determining the conversion between TCC and irradiance. As degradation is often exponential in nature, the calibration trend is modeled as an exponential. The ratio of TCC to expected irradiance is modeled as

$$\frac{TCC}{E} = a \cdot e^{-\tau \cdot t} + b, \tag{2}$$

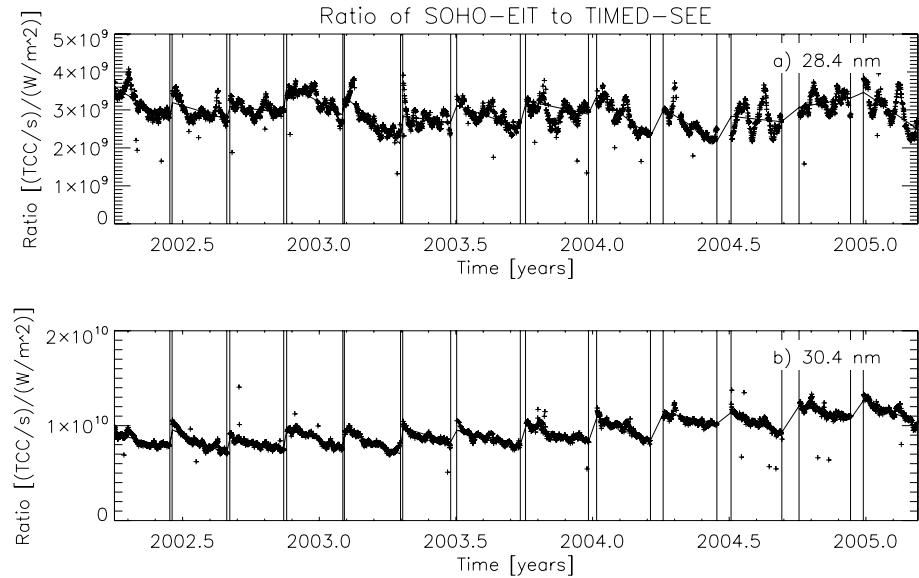


Figure 5 Ratio of EIT TCC to SEE irradiance for (a) the 28.4-nm channel and (b) the 30.4-nm channel. The vertical lines mark the start and end of EIT bakeouts. The solid lines are the exponential fit to the ratio between each EIT bakeout.

where E is the SEE irradiance convolved with the EIT responsivity and TCC is the EIT TCC. The variables a , τ , and b are then fit independently for each period between bakeouts by using a least-squares method. This gives a time-dependent calibration factor. The fitted EIT irradiance is therefore the EIT TCC divided by the cross-calibration factor.

3.4. Data Selection

To ensure that the best calibration is obtained of the EIT images, certain images are ignored in the fit. Sometimes, EIT has transmission errors where blocks of pixels are missing from data stream. As these missing blocks affect the total counts, images with missing blocks are omitted.

Furthermore, images with a large number of particle hits are ignored. EIT processing corrects for particles by replacing unusually high pixel values with the median of surrounding pixels. For “snowy” images with many particle hits, this method is not effective as one bad pixel is being replaced by another. As a result, images that have more than 1.5% high-valued pixels are ignored.

3.5. Uncertainties in Fit

Uncertainties in the fit are difficult to obtain. As we are fitting EIT to SEE, the SEE data are assumed to be the “true” irradiance. However, SEE has well-understood uncertainties of order of 30% in the EIT spectral range (Figure 1(b)). EIT uncertainties are harder to calculate as the total error budget is given as roughly 70% based primarily on pre-flight calibrations (Dere *et al.*, 2000) and has no time dependence. Since the total count value for individual images is on the order of 10^5 , the random error for the TCC is less than 0.5%. For this

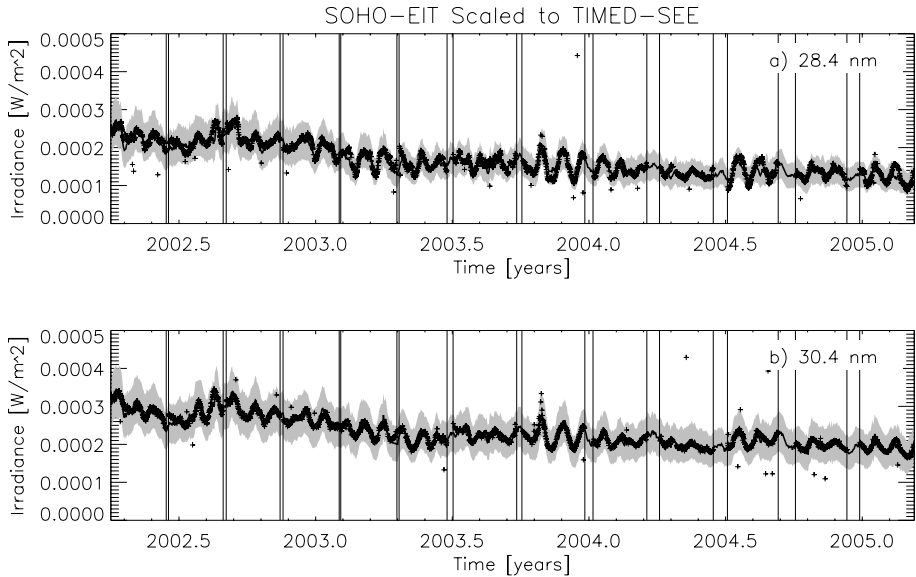


Figure 6 Results of the cross-calibration for (a) the 28.4-nm channel and (b) the 30.4-nm channel, showing the calibrated EIT irradiances (+) and the SEE data (solid lines). Also shown are the uncertainty in the SEE data (shaded area) and the start and end of the EIT bakeouts (vertical lines).

analysis, the convolved SEE uncertainties, calculated by convolving the SEE uncertainties and the EIT responsivities, are used as a measure of how good the calibration is.

4. Cross-Calibration Results and Discussion

The results of the cross-calibration applied to the EIT TCC are shown in Figure 6; Figure 7 gives the residuals (the ratio of the difference of the fitted EIT and SEE measurements to the SEE measurements). The fitted EIT irradiance successfully follows the variability of SEE on both solar rotation and yearly time scales. The residuals are, in general, within the error of the SEE irradiance measurements.

4.1. Comparison across Channels

Overall, the 30.4-nm data have smaller residuals than the 28.4-nm data and the 30.4-nm channel is more sensitive to CCD changes than the 28.4-nm channel. There are at least three potential reasons for this. First, the 30.4-nm channel is dominated by one line whereas the 28.4-nm channel has several strong lines. If the EIT bandpasses are not correct, the relative contributions from lines in the 28.4-nm channel could be incorrect, which would affect the convolved SEE irradiance. Second, the dominant line in the 30.4-nm channel is a He II line that is formed at a lower temperature than the Fe XV line in the 28.4-nm channel. For solar spectral irradiance emerging from the transition region and corona, the variability increases as the temperature of the emitting plasma also increases. As a result, the CCD degradation in the 28.4-nm channel is masked by larger changes in the Sun while the degradation dominates the 30.4-nm channel. For this reason, it is easier to fit the 30.4-nm channel than the 28.4-nm channel. Lastly, the uncertainty in SEE irradiance data increases at shorter wavelengths.

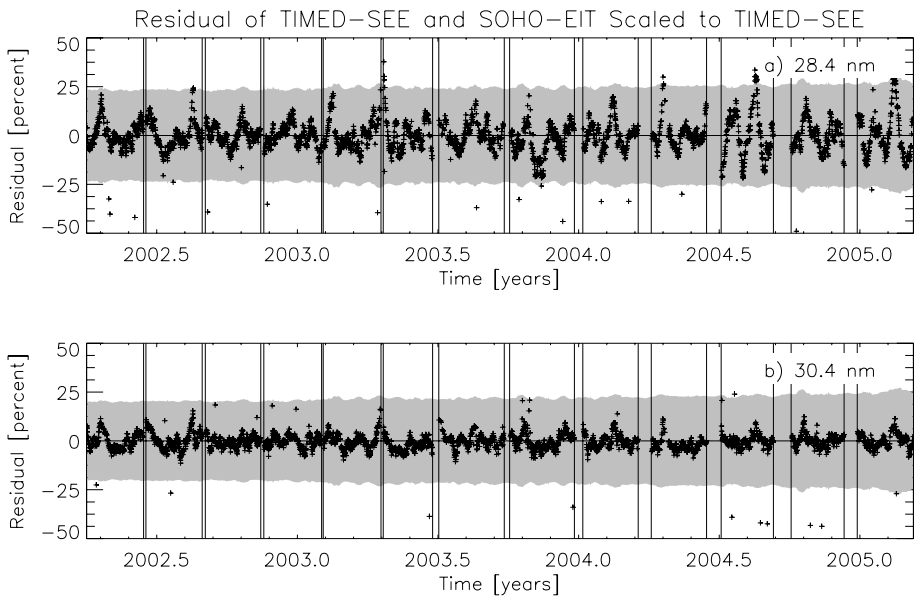


Figure 7 Residuals of cross-calibration for (a) the 28.4-nm channel and (b) the 30.4-nm channel, showing the ratio of the calibrated EIT irradiances and SEE data (+). The shaded areas are the uncertainty in the SEE data; the vertical lines mark the start and end of EIT bakeouts.

4.2. Field-of-View Considerations

Another factor influencing the size of the residuals is the difference in field of view (FOV) for EIT and SEE. SEE had a FOV of 6° by 12° whereas EIT has a $45'$ by $45'$ FOV. As a result, if there are coronal emissions that occur beyond $\approx 1.5R_\odot$, they will be detected by SEE but not by EIT. FOV effects should be more evident in the 28.4-nm channel than the 30.4-nm channel as the 28.4-nm channel images a hotter part of the corona, which is higher in the corona and thus appears farther from the solar limb in EIT images.

In general, there are larger residuals when the solar rotation cycle is stronger. The large residuals in the 28.4-nm channel during the later half of 2004 may be a result of solar activity occurring outside EIT's FOV. To better understand the importance of this effect, EIT 28.4-nm channel images were calibrated including only pixels within $1.0R_\odot$, $1.2R_\odot$, and $1.4R_\odot$. Figure 8 shows the cross-calibration residuals, which decrease as more of the solar corona is included. The standard deviation of $r < 1.0R_\odot$ is 17.5 whereas the standard deviation of $r < 1.2R_\odot$ is 9.7 and the standard deviation of $r < 1.4R_\odot$ is 8.5. The 10% decrease between the standard deviation of the residuals for $r < 1.2R_\odot$ and $r < 1.4R_\odot$ is not insignificant.

4.3. Comparison to EIT Calibrated with the SUSIM Mg II Index

Finally, we compare this new calibration using SEE irradiances with the current calibration using the SUSIM Mg II index to determine whether the two calibrations differ. To do this we reprocess all the EIT images, this time including the Mg II calibration, which is provided in SolarSoftWare by the EIT team. The TCC is calculated as before by totaling the counts from each pixel. As the Mg II index does not provide physical units, the Mg II-calibrated

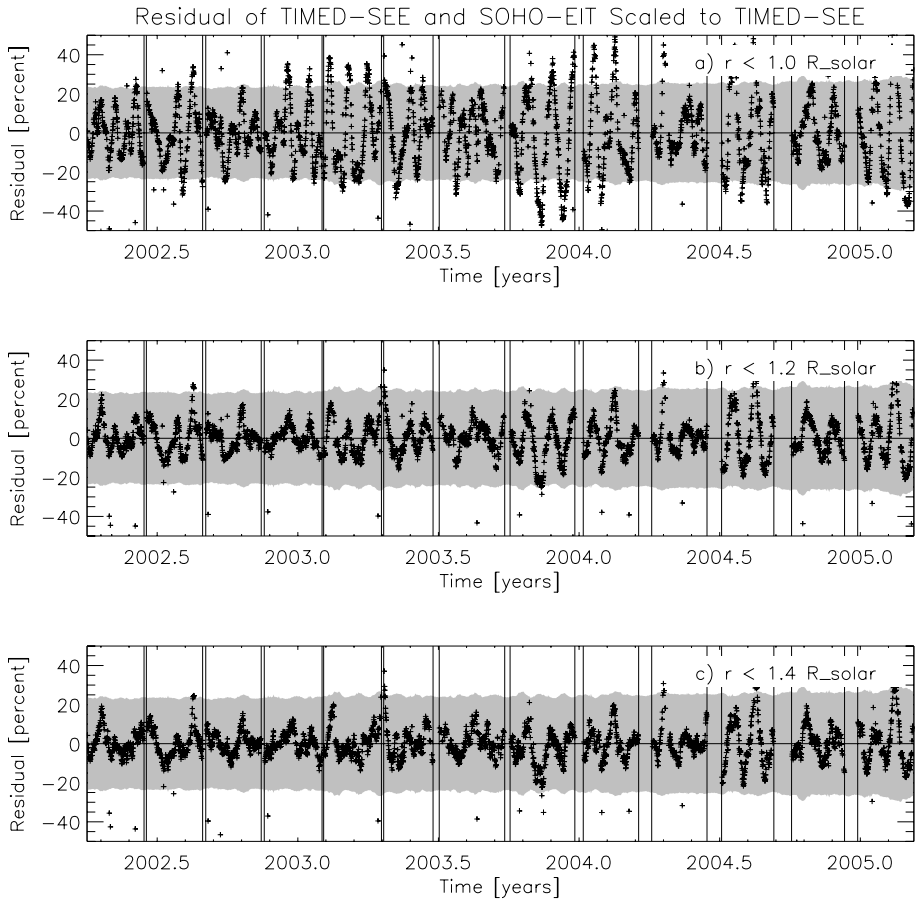


Figure 8 Residuals of cross-calibration for the 28.4-nm channel including only pixels within (a) $1.0R_{\odot}$, (b) $1.2R_{\odot}$, and (c) $1.4R_{\odot}$ showing the ratio of the calibrated EIT irradiances and SEE data (+). The shaded areas are the error in the SEE data; the vertical lines mark the start and end of EIT bakeouts.

EIT TCC is scaled to the SEE irradiance for the first day of this study, 1 April 2002, to allow for easier comparison (Figures 9 and 10).

SEE-calibrated EIT irradiances, not surprisingly, are better able to match the SEE irradiance measurements than Mg II-calibrated EIT. However, the differences between the two calibration methods are within the uncertainties of both the SEE measurements (30%) and the EIT calibrations (70%). Furthermore, because the periods between bakeouts are only a few months long, it is difficult to separate differences in the calibrations resulting from solar rotation or cycle variations from those resulting from bakeout effects.

In fact, the Mg II calibration has a long-term trend in the residuals of -4.8% per year for the 28.4-nm images and 2.1% per year for the 30.4-nm images. For the SEE-calibrated irradiances, the long-term trend is -0.1% per year for both channels.

Furthermore, the SEE calibration is able to better match the solar rotation variability than the Mg II calibration. The residuals from the SEE-calibrated EIT irradiances have a standard deviation of 8.3% for the 28.4-nm images and 4.4% for the 30.4-nm images whereas the

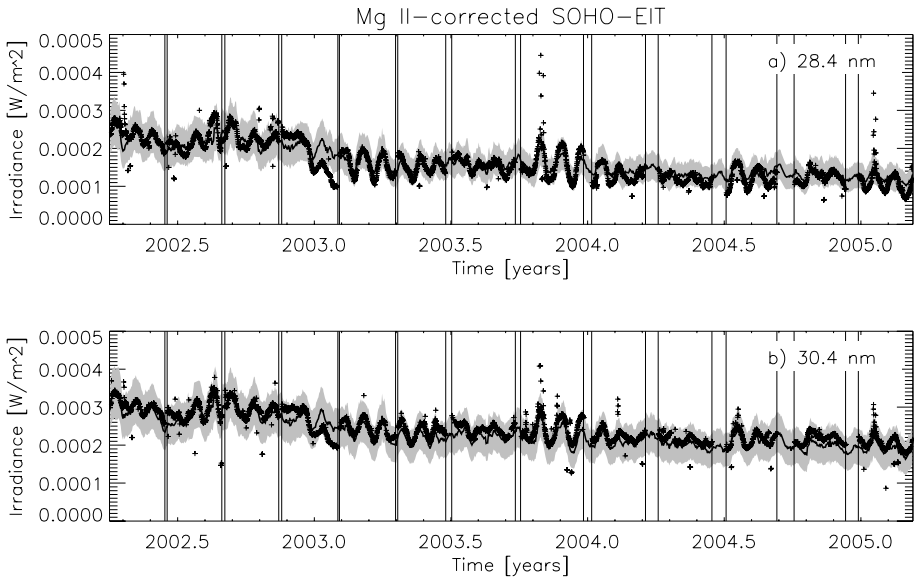


Figure 9 EIT irradiances calibrated with the Mg II index (+) for (a) the 28.4-nm channel and (b) the 30.4-nm channel. The solid lines are the convolved SEE irradiance; the shaded areas are the SEE uncertainty. The vertical lines mark the start and end of EIT bakeouts.

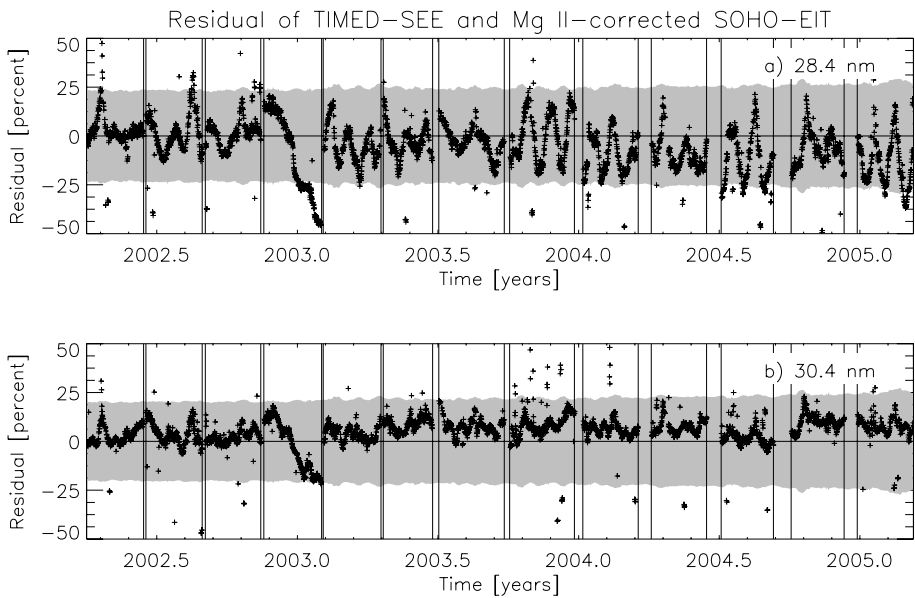


Figure 10 The residual of EIT calibrated with the Mg II index and SEE measurements for (a) the 28.4-nm channel and (b) the 30.4-nm channel. The shaded areas are the uncertainty in the SEE measurements and the vertical lines mark the start and end of EIT bakeouts.

residuals from the Mg II calibration have standard deviations of 12.9% and 7.9%, respectively. In addition, there is one period in late 2002 where the Mg II-calibrated EIT irradiance does not trend similarly to SEE irradiance data. This is not surprising because Mg II does not measure coronal emission. Coronal lines show different solar rotation variations than transition region or chromospheric lines.

4.4. Future Work

This work used less than a third of the available images for the 28.4- and 30.4-nm channels as SOHO was launched in late 1995 and we only analyzed images from mid-2002 though mid-2005. The cross-calibration can be extended to earlier portions of the SOHO mission by using a model such as the Flare Irradiance Spectral Model (FISM) (Chamberlin, Woods, and Eparvier, 2007) or the SOHO SEM 26–34 nm band. FISM is an empirical model of solar irradiance from 0.1 to 190 nm at 1-nm resolution based on SEE data. Because FISM contains spectral information, it can provide a better absolute calibration of EIT images prior to the launch of TIMED. Extending the time range would allow for further comment on the strengths and weaknesses of the current Mg II calibration. For example, the Mg II calibration may work better at solar maximum than it does at solar minimum.

This type of cross-calibration will be applied to SDO AIA solar images by using solar EUV spectra from SDO EVE. The higher time cadence, better spectral overlap, and higher accuracies of the two instruments will allow for an improved cross-calibration. Residuals from the cross-calibration may be able to be used to calculate changes to the AIA bandpasses from both contaminants and long-term degradation. This is not possible with EIT and SEE because our residuals were already within the uncertainties of SEE. Furthermore, the overlap in the SOHO and SDO missions will allow us to extend the cross-calibration back to the beginning of the SOHO mission through an improved FISM model.

5. Conclusions

EIT 28.4- and 30.4-nm channel images from 1 April 2002 to 15 March 2005 were absolutely calibrated by using SEE irradiance data convolved with the EIT bandpasses. This calibration provided both a correction for the long-term trends in the EIT CCD and a time-dependent correction factor to convert total image counts to irradiances. The residuals of the fit were well within the uncertainties of both SEE (30%) and EIT (70%). Moreover, there may be some contribution to the residuals from the different fields of view of the two instruments.

The results of this new calibration were compared to the currently used calibration based on the SUSIM Mg II index. Overall, the SEE-calibrated EIT irradiances correspond more closely with SEE irradiances than do the Mg II-calibrated EIT irradiances. The SEE calibration has a smaller spread of residuals and does not have the long-term trends that are seen in the Mg II calibration. Furthermore, this new calibration does provide physical units that are not determined by using the Mg II index.

Acknowledgements The SEE data products are available online at <http://lasp.colorado.edu/see/>. The EIT images are from the SOHO EIT Consortium; SOHO is a joint ESA and NASA program. This research is supported by NASA Contract No. NAS5-02140 to the University of Colorado.

References

- Chamberlin, P.C., Woods, T.N., Eparvier, F.G.: 2007, *Space Weather* **5**, 7005.
- Clette, F., Hochedez, J.-F., Newmark, J.S., Moses, J.D., Auchère, F., Defise, J.-M., Delaboudinière, J.-P.: 2002, In: Pauluhn, A., Huber, M.C.E., von Steiger, R. (eds.) *The Radiometric Calibration of SOHO*, **SR-002**, ESA, Noordwijk, 121.
- Dere, K.P., Moses, J.D., Delaboudinière, J.-P., Brunaud, J., Carabetian, C., Hochedez, J.-F., *et al.*: 2000, *Solar Phys.* **195**, 13.
- Floyd, L., Newmark, J., Cook, J., Herring, L., McMullin, D.: 2005, *J. Atmos. Solar-Terr. Phys.* **67**, 3.
- Newmark, J.S., Moses, J.D., Cook, J.W., Delaboudiniere, J.-P., Song, X., Carabetian, C., *et al.*: 2000, In: Fineschi, S., Korendyke, C.M., Siegmund, O.H., Woodgate, B.E. (eds.) *Instrumentation for UV/EUV Astronomy and Solar Missions*, *Proc. SPIE* **4139**, 328.
- Woods, T.N., Eparvier, F.G., Bailey, S.M., Chamberlin, P.C., Lean, J., Rottman, G.J., Solomon, S.C., Tobiska, W.K., Woodraska, D.L.: 2005, *J. Geophys. Res. A* **110**, 1312.